Pergamon

0301-9322(93)E0001-L

Int. J. Multiphase Flow Vol. 20, No. 1, pp. 81–98, 1994

0301-9322/94 $6.00 + 0.00

EXPERIMENTAL MEASUREMENTS IN A DUSTY-GAS SHOCK TUBE

G. D. Lock†

Institute for Aerospace Studies, University of Toronto, 4925 Dufferin St, Downsview, Ontario, Canada M3H 5T6

(Received 16 March 1993; in revised form 10 October 1993)

Abstract—A dusty-gas shock tube has been used to experimentally investigate the structure of a normal shock wave in steady one-dimensional dusty-gas flows. The investigation includes: direct and indirect measurements of the pressure, gas- and particulate-phase velocities and concentrations in the initial equilibrium region before the shock arrival; measurements of the changes in these properties across the shock front; measurements of these properties in the final equilibrium region; and measurements of the variations of these properties as a function of time through the relaxation zone that separates these initial and final equilibrium regions. Results of these experiments show that the thermodynamic variables follow the trends predicted by two-phase theory, but generally reach equilibrium in a shorter relaxation time than that predicted by computations using the standard drag coefficient.

Key Words: shock tube, shock wave, dusty gas

INTRODUCTION

Moving gases containing a suspension of solid particles are normally called gas–particulate or dusty-gas flows (Soo 1967; Rudinger 1980). Such two-phase flows occur in nature (haze, smoke and volcanic-ash clouds; sand and hail storms), and they are common to industrial engineering (fluidized beds, material conveyance, atmospheric migration of pollutants, air-quality control), to aerospace engineering (solid-propellant rocket motors, aerodynamics of flight in a dusty-gas environment, particle erosion of spacecraft and jet-engine compressor blades) and also to explosions (coal mines, grain elevators, military). Many of these dusty-gas flows contain shock waves with non-equilibrium flow regions. Stationary and moving shocks produce relative motion and temperature differences between the gas and particulate phases, and the resulting viscous drag and heat transfer between these phases act to establish equilibrium. Both theoretical and experimental investigations of these flows provide much insight into two-phase flow phenomena, better industrial and aerodynamic design and increased safety.

Studies of shock-induced dusty-gas flows date back to the 1950s. The long lists of references given by Soo (1967) and Rudinger (1980) indicate extensive theoretical, numerical and experimental activities in this field. However, the theoretical and numerical contributions far outnumber the experimental ones. Experimental work has been performed in the areas of shock-wave decay and unsteadiness (Sommerfeld & Grönig 1983; Sommerfeld 1985), drag-coefficient measurements (Rudinger 1963, 1970; Buckley 1970; Selberg & Nicholls 1968), the structure of a normal shock wave (Outa *et al.* 1976, 1981; Hongru *et al.* 1985; Sugiyama *et al.* 1985), concentration measurements with light extinctiometry and β-ray densitometry (Lock & Gottlieb 1989), indirect gas- and particle-velocity measurements (Lock & Gottlieb 1990), shock-induced boundary-layer dust lofting (Batt *et al.* 1987), shock reflections (Sommerfeld *et al.* 1985; Suzuki *et al.* 1989), density measurements in blast waves with dust (Frank & Saint 1984; Ritzel 1985) and the influence of solid particles on supersonic jets (Sommerfeld 1989).

In the work described in this paper, a dusty-gas shock tube has been used to experimentally investigate the structure of a normal shock wave in a steady one-dimensional dusty-gas flows. The investigation includes: direct and indirect measurements of the pressure and gas- and particulate-

†Present address: Oriel College and Department of Engineering Science, Oxford University, Oxford OX1 4EW, England.

phase velocities and concentrations in the initial equilibrium region before the shock arrival; measurements of the changes of these properties across the shock front; measurements of these properties in the final equilibrium region; and measurements of the variations of these properties as a function of time through the relaxation zone that separates these initial and final equilibrium regions. Wherever possible these measurements are compared with the results predicted by two-phase flow theory. These experiments have also led to measurements of the drag coefficient governing the dynamic interaction between the gas and particulate phases. This drag coefficient is correlated with the Reynolds number and compared with results obtained by other authors.

NON-EQUILIBRIUM SHOCK STRUCTURE IN A DUSTY GAS

Some of the measurement techniques for shock-induced dusty-gas flows, including those used in the work presented herein, are restricted in application to the case of shock waves which have a stationary shock structure. Consider a shock-tube experiment in which a shock wave is moving at a constant speed, V^s, along a constant-area duct containing a dusty gas. Before the arrival of the shock front at the test or measurement section, let the gas and particles be in thermal and kinematic equilibrium ($T_G = T_p$ and $v_G = v_p$, where these symbols represent the gas and particulate temperatures and velocities, respectively, with the velocities measured in the laboratory frame of reference). The two phases may be at rest or in steady motion. As this shock wave passes the test section, the gas properties therein increase very rapidly across the shock front from their initial equilibrium state (i) ahead of the shock to their new frozen state (f) just behind the shock front ($T_{Gf} > T_{Gi}; v_{Gf} > v_{Gi}$). This is illustrated in figure 1. The solid particles do not experience an abrupt change in velocity or temperature across the shock front (owing to their mass and thermal inertia) and, therefore, in the frozen state and the following non-equilibrium flow region there exist differences in the thermal and kinematic properties of the gas and particles ($T_G > T_p; v_G > v_p$). The non-equilibrium velocity and temperature differences produce aerodynamic drag and heat transfer between the two phases, both which act to establish a new equilibrium state (e) at some later time. Both phases exhibit increases in velocity, temperature and other flow properties through the non-equilibrium flow region. Although the particulate and gas velocities increase in a monotonic manner as shown, the gas temperature may exhibit a maximum or minimum. Also, the final equilibrium gas temperature may be higher or lower than the frozen value, depending on the shock Mach number and the dust-to-air loading ratio. The non-equilibrium shock structure depicted in figure 1 is for a partly dispersed shock wave. Under certain flow conditions the entire non-equilibrium transition may occur without a discontinuity in the gas phase, and this would be the case for a fully dispersed shock wave (Outa *et al.* 1976; Sommerfeld 1985).

The concentrations of the gas and particulate phases (σ_G and σ_p) exhibit similar trends to those illustrated in figure 1, except that in the equilibrium regions the gas and particulate-phase concentration need not equal each other but are constant with respect to time. The particulate concentration is the amount of particle mass per unit volume of mixture, which is distinct from the larger particle material density ρ_p. Let ζ denote the volume fraction of the particle material in the mixture, and then $\sigma_p = \zeta\rho_p$. Similarly, there is a distinction between the gas density ρ_G and the gas concentration $\sigma_G = (1 - \zeta)\rho_G$. From these definitions it follows that the mixture concentration (which is equivalent to the mixture density) is given by the sum $\sigma_m = \sigma_p + \sigma_G$. Note that the particle volume fraction for typical gas–particulate flows is small ($\zeta \sim 10^{-3}$) because $\rho_G \ll \rho_p$, and in this case the gas concentration and density are nearly equal (and often considered synonymous).

The flow properties presented in figure 1 correspond to the particular case of a stationary shock structure. As a shock wave moves along a duct at a constant velocity, a Galilean transformation can be performed to result in a steady flow for an observer moving with the wave. The transformed flow field does not depend explicitly on time and the entire relaxation process can be considered stationary.

Shock waves with a stationary structure are not produced immediately in shock tubes, but they are the final product of an evolutionary process. Normally an unsteady shock wave with a varying propagation speed and changing flow-property structure evolves into one which moves at a

constant speed and has a fixed structure. For example, a flat-topped shock wave moving initially in a gaseous medium would undergo complicated wave reflection and refraction processes on entering and traversing a dusty gas (Miura & Glass 1983), and these processes would alter the shock wave's speed and structure towards the final stationary state (with a partly or fully dispersed structure). These events also occur when a shock wave is produced in a dusty-gas shock tube by the breaking of a diaphragm between the high and low pressure chambers (Outa *et al.* 1976; Miura & Glass 1982; Sommerfeld & Grönig 1983; Sommerfeld 1985), and also when a shock wave is produced in front of a piston which is set in impulsive motion to a constant velocity (Miura & Glass 1985).

FROZEN-, EQUILIBRIUM- AND NON-EQUILIBRIUM-FLOW CALCULATIONS

The solution to the changes in the thermodynamic properties of the gas and particulate phases between the initial equilibrium, frozen and final equilibrium states for the flow induced by the passage of a normal shock wave with stationary structure has been well-documented (Rudinger 1980). These solutions are obtained by solving the equations of conservation of mass, momentum and energy for both phases in conjunction with the equation of state.

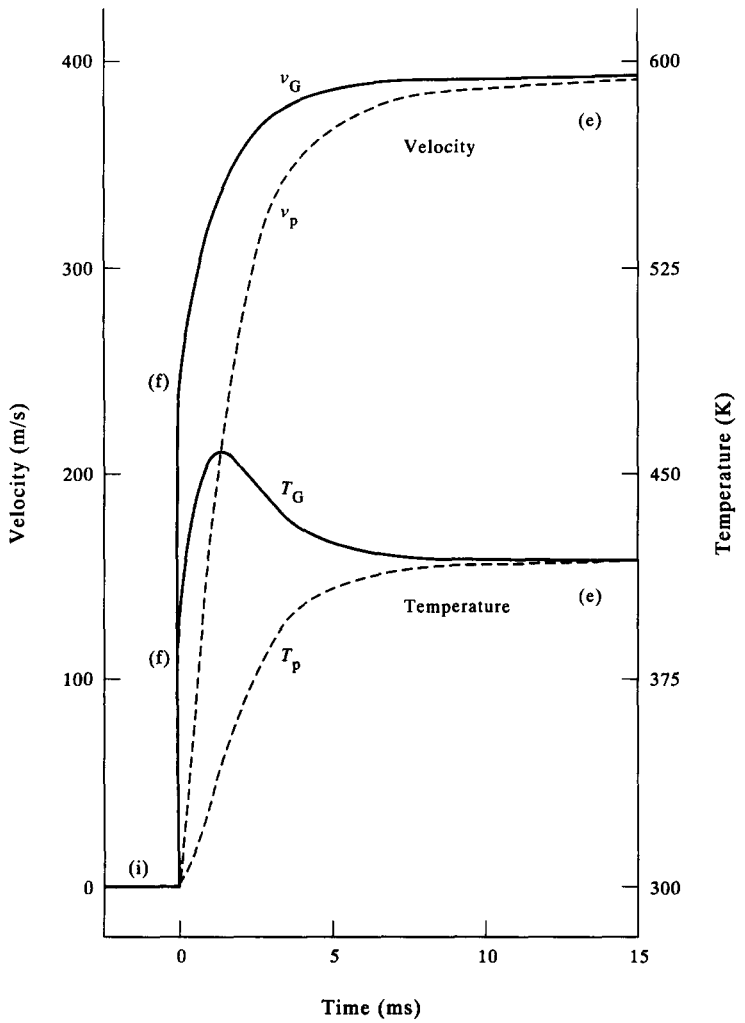

Figure 1. Gas- and particulate-phase velocity and temperature variations with time through a shock wave with a stationary structure in a dusty gas.

Frozen-flow conditions

The time in which a particle crosses the shock front is approximately equal to D/V_s, where D is the particle diameter. For $D < 100\,\mu$m, this time is negligible in comparison with the relaxation time and so the particle crosses the shock front with negligible changes in velocity and temperature. It should be noted that a small change in velocity does occur due to the effects of virtual mass (Rudinger 1965), but for $\rho_G/\rho_p \sim 10^{-3}$ this jump is insignificantly small (Gottlieb & Coskunses 1985). If the particle velocity is not changed during the passage across the shock front, then the particle spacing, and therefore the volume fraction is conserved; thus $\zeta_i = \zeta_f$ and the conditions of the particulate phase immediately downstream of the shock are essentially the same as those upstream of the shock, viz.

$$\sigma_{pi} = \sigma_{pf} \quad [1]$$

$$T_{pi} = T_{pf} \quad [2]$$

and

$$v_{pi} = v_{pf}. \quad [3]$$

Therefore they may be omitted from the conservation equations if the corresponding conditions in the gas are to be solved. One is then left with the equations that describe the conservation of mass, momentum and energy for a dust-free gas. The solution is given by the well-known Rankine–Hugoniot equations which are listed as follows:

$$\frac{V_s - v_{Gi}}{V_s - v_{Gf}} = \frac{\rho_{Gf}}{\rho_{Gi}} = \frac{\sigma_{Gf}}{\sigma_{Gi}} = \frac{(\gamma+1)M_{sf}^2}{(\gamma-1)M_{sf}^2 + 2}, \quad [4]$$

$$\frac{p_f}{p_i} = \frac{2\gamma}{\alpha g + 1}(M_{sf}^2 - 1) + 1 \quad [5]$$

and

$$\frac{T_{gf}}{T_{Gi}} = \left(\frac{p_f}{p_i}\right)\left(\frac{\sigma_{Gi}}{\sigma_{Gf}}\right), \quad [6]$$

where p denotes the gas pressure, unaffected by the particulate phase (Rudinger 1980), γ is the ratio of specific heats for air and $M_{sf} = V_s/a_f = V_s/\sqrt{(\gamma R T_i)(1-\zeta)^{-1}}$ is the frozen shock Mach number with a_f representing the frozen sound speed in the dusty-gas mixture and R the gas constant for air. The frozen conditions immediately behind the shock front are thus completely determined if the initial conditions and frozen shock Mach number are prescribed.

The small effect of virtual mass has been ignored in the above solutions. The effect of the virtual mass on the frozen conditions of both the gas and particles has been documented by Gottlieb & Coskunses (1985). A coefficient of virtual mass appears in all of the frozen-flow solutions, which reduce to the above equations if this coefficient is set to zero.

Equilibrium-flow conditions

The flow properties in the final equilibrium region behind the relaxation region of a shock wave in a dusty gas can be determined analytically by equating the gas- and particulate-phase velocities and temperatures ($v_{Ge} = v_{pe}$ and $T_{ge} = T_{pc}$) in the conservation equations. A closed-form solution was obtained by Rudinger (1965) in terms of the equilibrium shock Mach number. This solution is expressed as follows:

$$\frac{V_s - v_{Gi}}{V_s - v_{Ge}} = \frac{V_s - v_{pi}}{V_s - v_{pe}} = \frac{\sigma_{Ge}}{\sigma_{Gi}} = \frac{\sigma_{pe}}{\sigma_{pi}} = \frac{\zeta_e}{\zeta_i} = \frac{(\Gamma+1)M_{se}^2}{(\Gamma-1)M_{se}^2 + 2 + 2\zeta_i(M_{se}^2 - 1)}, \quad [7]$$

$$\frac{\rho_{Ge}}{\rho_{Gi}} = \frac{\sigma_{Ge}(1-\zeta_i)}{\sigma_{Gi}(1-\zeta_e)}, \quad [8]$$

$$\frac{p_e}{p_i} = \frac{2\Gamma}{\Gamma+1}(M_{se}^2 - 1) + 1 \quad [9]$$

and

$$\frac{T_{Ge}}{T_{Gi}} = \frac{T_{pe}}{T_{pi}} = \left(\frac{p_e}{p_i}\right)\left(\frac{\rho_{Gi}}{\rho_{Ge}}\right), \qquad [10]$$

with

$$M_{se} = M_{sf}\sqrt{\frac{(1+\eta)(1+\gamma\eta\delta)}{1+\eta\delta}} \quad \text{and} \quad \Gamma = \frac{\gamma(1+\eta\delta)}{1+\gamma\eta\delta}.$$

In these expressions, M_{se} is the equilibrium shock Mach number, δ is the specific heat of the particle material divided by the gas specific heat at constant pressure, Γ is an equilibrium specific heats ratio and the particle-to-air loading ratio is given by $\eta = \sigma_{pi}/\sigma_{Gi}$. For $\zeta = 0$, the above equations become the standard Rankine–Hugoniot relations, [4]–[6], for a Mach number M_{se} and a specific heat ratio Γ.

Non-equilibrium-flow conditions

The flow properties in the relaxation zone, between the frozen and final equilibrium regions, cannot be solved exactly in analytical form. Consequently, the relevant equations are solved numerically. Numerous such solutions can be found in the literature (e.g. Carrier 1958; Kriebel 1964; Rudinger 1964; Soo 1967; Marble 1970). The different authors used different assumptions in their analyses as well as different expressions for the drag and heat-transfer coefficients. Kriebel (1964) used the drag-coefficient given by $C_d = 24/\mathrm{Re}(1 + \mathrm{Re}^{2/3}/6)$ and a Nusselt number given by $\mathrm{Nu} = C_d\,\mathrm{Re}/12$. Marble (1970) used the Stokes drag and a constant $\mathrm{Nu} = 1$. Rudinger (1964) illustrated the effects on the relaxation profile of varying the different drag and heat-transfer correlations. The three drag correlations he used are given by Stokes drag, the expression $C_d = 28/\mathrm{Re}^{0.85} + 0.48$, and the accelerated drag coefficients obtained experimentally by Ingebo (1956). The two Nu correlations he used were $\mathrm{Nu} = 2$ and $\mathrm{Nu} = 2 + 0.6\,\mathrm{Pr}^{1/3}\,\mathrm{Re}^{1/3}$.

The above references all assumed that the particle volume fraction ζ was negligible. Gottlieb & Coskunses (1985) included the effects of finite ζ and used the modified Henderson drag coefficient (Henderson 1978) and the correlated Nu correlation (Clift *et al.* 1978), which includes the effects of compressibility. It should be noted that for the small relative Mach numbers, defined by $(v_G - v_p)/a_f$, appearing in this paper these compressibility effects are negligible and the drag coefficient correlation is essentially the standard correlation (e.g. Schlichting 1968). The relaxation profiles obtained in this paper (see figure 9) are computed using the Fortran program listed in appendix C of the report by Gottlieb & Coskunses (1985). The method of solution and numerical technique used, a fourth-order Runge–Kutta scheme, are outlined in detail in the aforementioned report.

DUSTY-GAS SHOCK-TUBE FACILITY

The dusty-gas shock tube at the University of Toronto Institute for Aerospace Studies (UTIAS) is a laboratory tool used for conducting experimental studies of gas–particulate flows induced by shock waves. The facility is unique to other dusty-gas shock tubes in 4 repsects: (i) it is horizontally oriented; (ii) it has a large cross-sectional area; (iii) it has a long length of channel between the beginning of the dust cloud and the test section; and (iv) it has extensive instrumentation capabilities.

A schematic diagram of the shock tube with its dust-injection system is illustrated in figure 2. The driver is 2.43 m long and 21.2 cm dia, and the channel has a rectangular cross-section of 19.7 × 7.6 cm. The test section is located 9 m from the diaphragm. With plastic diaphragms the shock tube has been used to produce weak shock waves with frozen shock Mach numbers of $M_{sf} < 2$. Typical test times or non-equilibrium relaxations from the shock-front arrival at the test section to later in the flow are 1–10 ms. Detailed descriptions of the facility are available from a laboratory report (Czerwinski *et al.* 1987) and a thesis (Lock 1991).

A uniform dust–air mixture is created in the shock-tube channel by air injection from a high-pressure (690 kPa) reservoir. This special air reservoir, a dust chamber, control valve and pipe

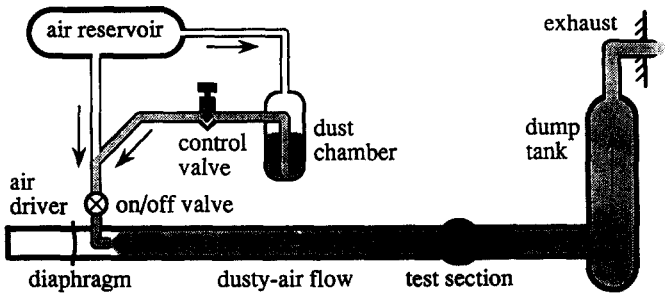

Figure 2. Schematic diagram of the UTIAS dusty-gas shock-tube facility with its dust-injection system.

junction are used to mix the air and dust before injection via a 3 cm dia nozzle into the channel. The premixed air and dust (40 μm glass spheres) are injected near the diaphragm station, along the channel and through the test section into the dump tank, at a speed of approx. 25–30 m/s, 2–5 s before the shock-tube diaphragm is broken (see figure 3). The shock wave therefore travels down the channel superimposed on the dusty-gas flow. The shock must propagate through the initially supersonic expanding jet flow emanating from the injection nozzle, and then as it travels farther down the channel it evolves into a partly dispersed shock wave having a constant speed and stationary structure, before reaching the test section.

INSTRUMENTATION AND INDIRECT MEASUREMENT TECHNIQUES

To fully analyse the structure of a shock wave in a dusty gas experimentally, a number of fundamental gas- and particulate-phase properties must be measured. The UTIAS dusty-gas shock-tube facility has the instrumentation capable of performing these measurements. This instrumentation includes a laser-Doppler velocimeter (LDV), a light extinctiometer, a β-ray densitometer and a set of standard, commercial pressure transducers. This instrumentation, and indirect techniques using measurements from it, will be briefly discussed in this section.

A dual-beam LDV system operating in the forward-scatter mode is used to measure the particulate-phase velocity. Most of this system was assembled with standard TSI modular optics. The coherent laser light ($\lambda = 514.5$ mm) is provided by a Spectra Physics model 2000 argon-ion laser, operating at 0.5 W. The laser beams pass through a set of optical-quality glass windows and form an ellipsoidal probe volume at the shock-tube centreline. The probe-volume lengths on the major and minor axes are 4.20 and 0.173 mm, respectively. The interference-fringe spacing in the probe volume is 6.27 μm.

The LDV signals were amplified from a photomultiplier and sent to a TSI model 1990 counter. This counter operated in the *N cycle mode* so that the Doppler frequency was obtained by measuring the time between two voltage level settings. For all experiments $N = 8$, thus only Doppler bursts with at least 8 valid upper and lower trigger level crossings (set at 50 mV and 1 V) were accepted. To reduce erroneous velocity measurements from signals originating from more than one particle in the control volume, a measurement of the time taken for the first 4 pulses was compared with the time taken for all 8. If the pulse frequencies did not agree within 7% the measurement was rejected.

A light extinctiometer and β-ray densitometer are currently used in the dusty-gas shock-tube experiments to obtain the particle concentration σ_p and gas–particle mixture concentration σ_m, respectively. From these two measurements one can then calculate the gas concentration as $\sigma_G = \sigma_m - \sigma_p$. A description of these instruments and how they function has been reported previously (Lock & Gottlieb 1989; Lock 1991) and will not be reproduced here. However, it is worth mentioning that the β-ray densitometer does not give a straightforward value of σ_m for dusty-gas flows, as it would for gaseous flows only. Instead, it gives only an apparent concentration denoted as σ_m^{app}, and this value depends on the particle diameter and β-ray densitometer geometry. One has to first convert σ_m^{app} into a true α_m before the gas concentration can be obtained as outlined above. This conversion of σ_m^{app} into σ_m requires certain precautions and a special calibration of the β-ray densitometer with a dusty-gas flow (Lock & Gottlieb 1989). The

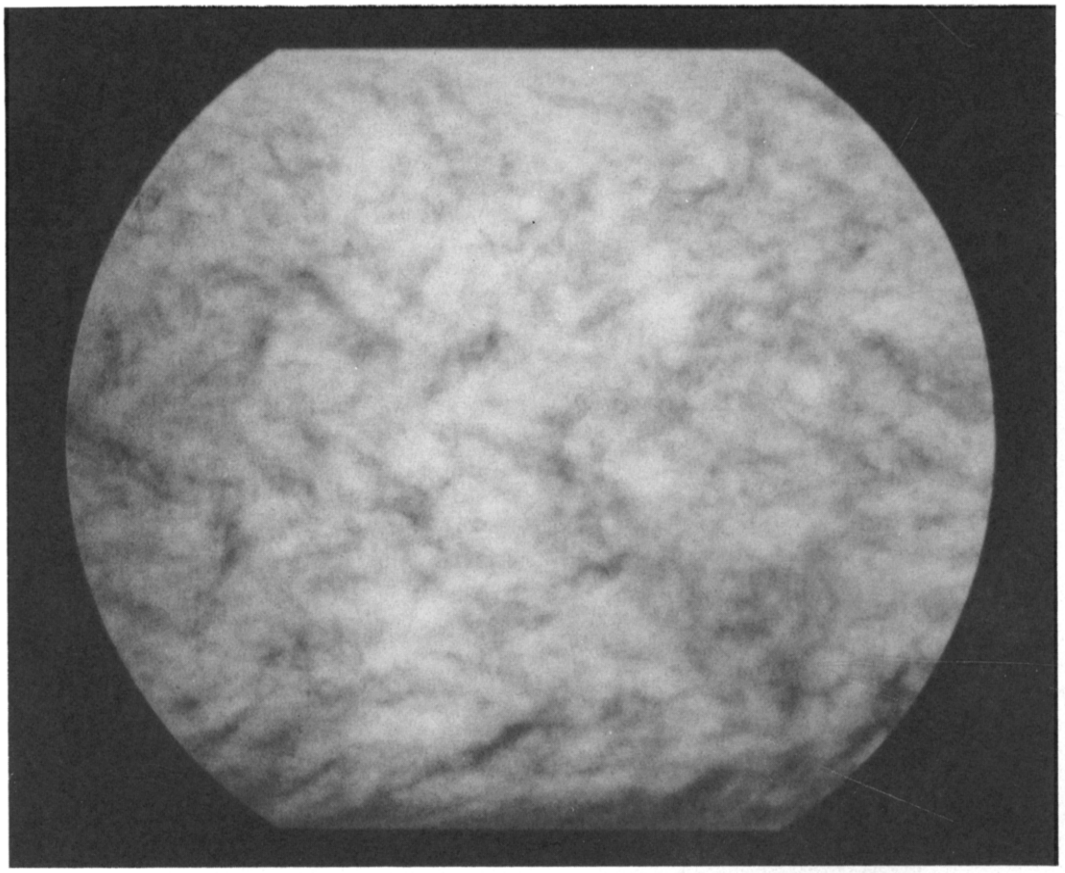

Figure 3. Photograph of an injected dust cloud. The flow is from left to right.

spatial resolution of the β-ray densitometer and light extinctiometer are 15.4 and 2 mm, respectively.

Pressure measurements are made with standard piezoelectric transducers. The shock-front velocity is also obtained from pressure measurements by averaging 5 time intervals for the shock front to traverse 5 equal distances between 6 equispaced pressure-sensitive transducers. In all experiments reported later the shock-front velocity remained essentially constant, within experimental uncertainty, over a distance of 6 m preceding the test section.

The instrumentation discussed above provides direct measurements of flow variables in a dusty-gas shock tube. From these measurements, other flow variables can be obtained indirectly by invoking known equations (e.g. equation of state, conservation of mass and momentum) applicable to the two-phase flow, as demonstrated by Rudinger (1963, 1970), Buckley (1970), Sommerfeld (1985) and Lock & Gottlieb (1990). These indirect measurements are restricted in application to the case of a stationary shock structure.

Two indirect velocity-measurement techniques are used in this work. The first of these utilizes the conservation of mass for both phases. For a shock wave with stationary shock structure, the conservation of mass for the gas and paritculate phases can be expressed as

$$\sigma_G(V_s - v_G) = \sigma_{Gi}(V_s - v_i) \qquad [11]$$

and

$$\sigma_p(V_s - v_p) = \sigma_{pi}(V_s - v_i). \qquad [12]$$

Hence, the values of v_G and v_p can be obtained indirectly by means of these two equations and the experimental measurements of V_s, σ_p and $\sigma_m = \sigma_p + \sigma_G$ with known initial conditions.

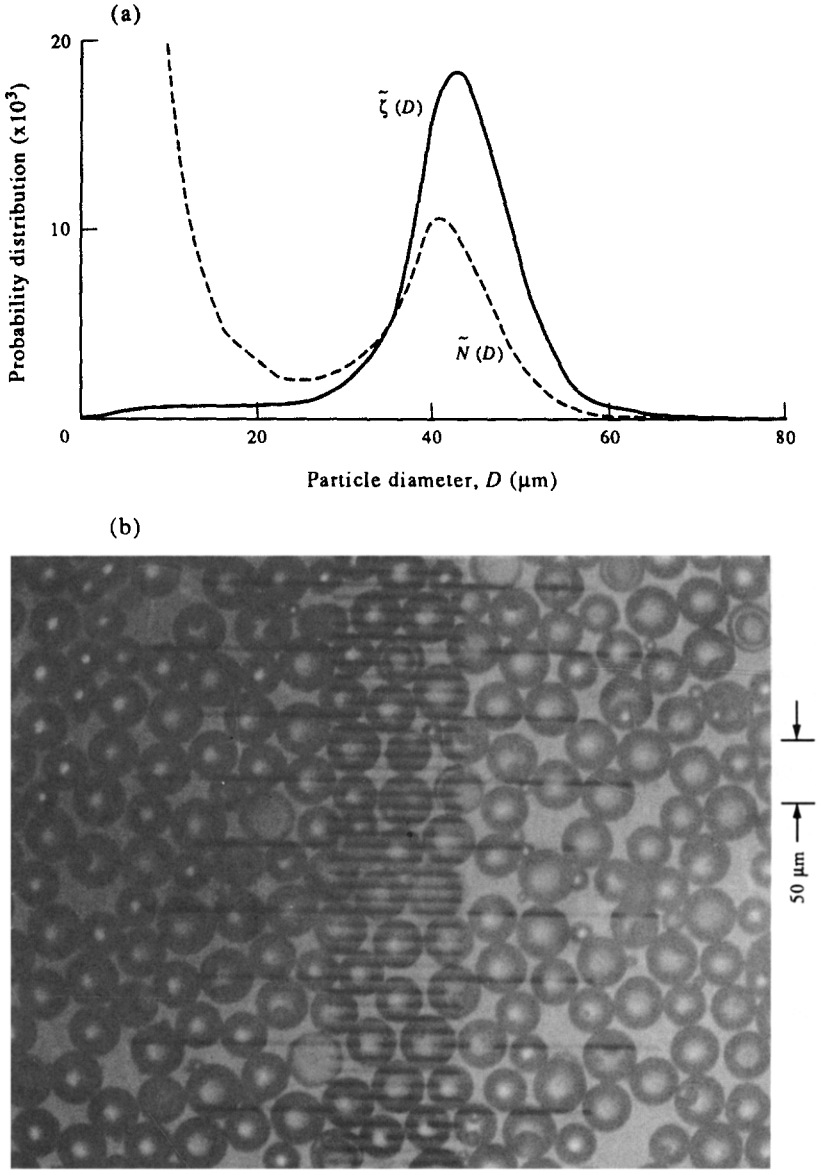

Figure 4. Microscope photograph of the glass beads (the major grid marks on the scale are 50 μm apart) and particle-size distributions on the basis of number $\tilde{N}(D)$ and volume $\tilde{\zeta}(D)$.

The second indirect method utilizes the conservation of mixture momentum. Combining the conservation equations of the mass of the gas and the particles and the momentum equation of the mixture for a negligible particle volume fraction ($\zeta \ll 1$), yields (Rudinger 1970):

$$(V_s - v_G) + \eta(V_s - v_p) + \frac{P}{\sigma_{Gi}(V_s - v_i)} = (1 + \eta)(V_s - v_i) + \frac{p_i}{\sigma_{Gi}(V_s - v_i)}. \quad [13]$$

If the particle concentration is known the particulate-phase velocity can be obtained indirectly from [12], as discussed above. (Alternatively the particulate-phase velocity may be obtained from direct LDV measurements.) Hence, the value of v_G can be obtained indirectly by means of [13] and the experimental measurements of V_s, σ_p and p. A detailed description of the indirect velocity-measurement techniques and how measurements using this technique with direct LDV measurements is given by Lock & Gottlieb (1990).

PARTICLES

The particles used in the experiments were glass microspheres (Ferro Corp., Standard U.S. mesh sieve size $-325+400$). These beams are manufactured from high-grade glass compounds and contain fewer than 2% irregular (non-spherical) particles. Liquid immersion tests at 298 K indicate an index of refraction of 1.51 and a material density $\rho_p = 2420\ \mathrm{kg/m^3}$. The particles are polysized and their probability density distributions by number and volume are denoted by $\tilde{N}(D)$ and $\tilde{\zeta}(D) = \tilde{N}D^3$. These distributions and a microscope slide of the particles are shown in figure 4. They are normalized so that $\int_0^\infty \tilde{\zeta}(D)\,\mathrm{d}D = 1$. These data were obtained from a Malvern series 2600c particle-size analyser (Monoresearch, Brampton, Canada), as well as from measurements taken from microscope slides. The data for $\tilde{\zeta}(D)$ illustrate that most particles are in a narrow diameter range near 40 μm, whereas the data for $\tilde{N}(D)$ indicates that numerous small particles are present in the samples for which $D < 20\ \mu$m. This is not serious because they do not contribute markedly to the overall mass and volume of the sample.

Only a small fraction of the particles that pass through the LDV probe volume produce a validated particle-velocity measurement. This is due partly to the validation criteria employed within the electronics but mostly due to the finite-signal amplitude range in which the LDV functions (Durst & Ruck 1987). The input signal to the LDV electronics was adjusted so that the larger particles set the highest signal amplitude possible in the Doppler-burst sequence entering the LDV electronics. A pre-set amplitide discrimination stage exists in the LDV electronics which sets a limit on the smallest-sized particle which can generate a valid signal. Only particles larger than about 15 μm constitute the effective particle-size range in the LDV experiments.

EXPERIMENTAL RESULTS AND DISCUSSION

Frozen-flow measurements

Experimental measurements of the pressure ratio (p_f/p_i) across the shock front of a normal shock wave with a stationary structure in a dusty gas are plotted as a function of the frozen shock Mach number M_{sf} in figure 5. The solid line in this figure is the pressure ratio predicted by two-phase theory, [5], and is seen to agree well with the experimental results over the range $1.05 < M_{sf} < 1.45$. The jump in pressure across the shock front is due to a compression of the gas phase only (this jump is independent of the loading ratio) and so only a single analytical curve is necessary despite slightly different initial conditions for each experiment.

Direct experimental measurements of the gas concentration ratio σ_{Gf}/σ_{Gi} (open circles) across the normal shock front are plotted as a function of the frozen shock Mach number M_{sf} in figure 6. Note that these *direct* concentration measurements lead to *indirect* measurements of the gas-phase velocity ratio across the shock fronts from [11]. Also plotted in this figure (solid circles) are the indirectly determined gas velocity ratios obtained from the conservation of mixture momentum, [13], and experimentally measured values of $p_f - p_i$, σ_{Gi}, $v_i = v_{Gi} = v_{pi}$ and V_s. The solid line in figure 6 is the gas concentration (or gas velocity) ratio calculated from two-phase theory and given by [4]. Again, these computed ratios were independent of the loading ratio and so only a single curve is present despite slightly different initial conditions upstream of the shock front.

Equilibrium-flow measurements

Experimental measurements of the pressure ratio between the final and initial equilibrium regions (p_e/p_i) for a normal shock wave with stationary structure in a dusty gas are plotted as a function of the equilibrium shock Mach number M_{se} in figure 7. Note that M_{se} is calculated from experimental measurements of M_{sf} and η. The loading ratio upstream of the shock front varied between $0.15 < \eta < 0.3$ for the experimental runs from which this data was obtained. For a particular value of M_{sf}, the pressure ratio p_e/p_i (unlike the pressure ratio p_f/p_i across the shock front) is a function of η, as is the value of M_{se}. The solid lines in this figure are the pressure ratios predicted by two-phase theory, [9], for $\eta = 0.15$ and 0.3. One observes that the experimentally obtained pressure ratios exhibit scatter yet follow the predicted theoretical trends over the range $1.25 < M_{se} < 1.17$, and are seen to increase as M_{se} increases.

Direct measurements of the gas- and particulate-phase velocity ratio, $(V_s - v_i)/(V_s - v_e)$ with

$v_e = v_{Ge} = v_{pe}$, between the initial and final equilibrium regions of a normal shock wave in a dusty gas are plotted as a function of the equilibrium shock Mach number M_{se} in figure 8. These measurements were obtained directly by means of the LDV at the test section of the dusty-gas shock tube. Direct measurements of the ratios of the particle concentration σ_{pe}/σ_{pi} (by means of the light extinctiometer) and the gas-phase concentration σ_{Ge}/σ_{pi} (by means of the light extinctiometer and β-ray densitometer) between the final and initial equilibrium regions are additionally plotted in this figure. Also appearing are the indirectly determined gas-phase velocity ratios obtained from the conservation of mixture momentum and experimentally measured values of $p_e - p_i$, σ_{Gi}, v_i, η and V_s, [13]. Plotted also in this figure (solid lines) are the velocity (or concentration) ratios calculated from two-phase theory, [7], for $\eta = 0.15$ and 0.3. All experiments were performed between these loading ratios.

The data in figure 8 exhibit scatter but generally follow the trends predicted by the two-phase theory. The 4 different experimental methods are shown to yield similar velocity and concentration ratios at equal M_s and are seen to increase as M_{se} increases, observations which are in accordance with two-phase theory.

Non-equilibrium-flow measurements

Figures 9(a–c) illustrate simultaneous measurements of the pressure (9a), gas- and particulate-phase concentrations (9b) and velocities (9c) for a typical experiment ($M_{sf} = 1.36$, $M_{se} = 1.60$, $\eta = 0.27$). These measurements were made at the test section of the dusty-gas shock tube, where the shock wave had obtained a stationary structure.

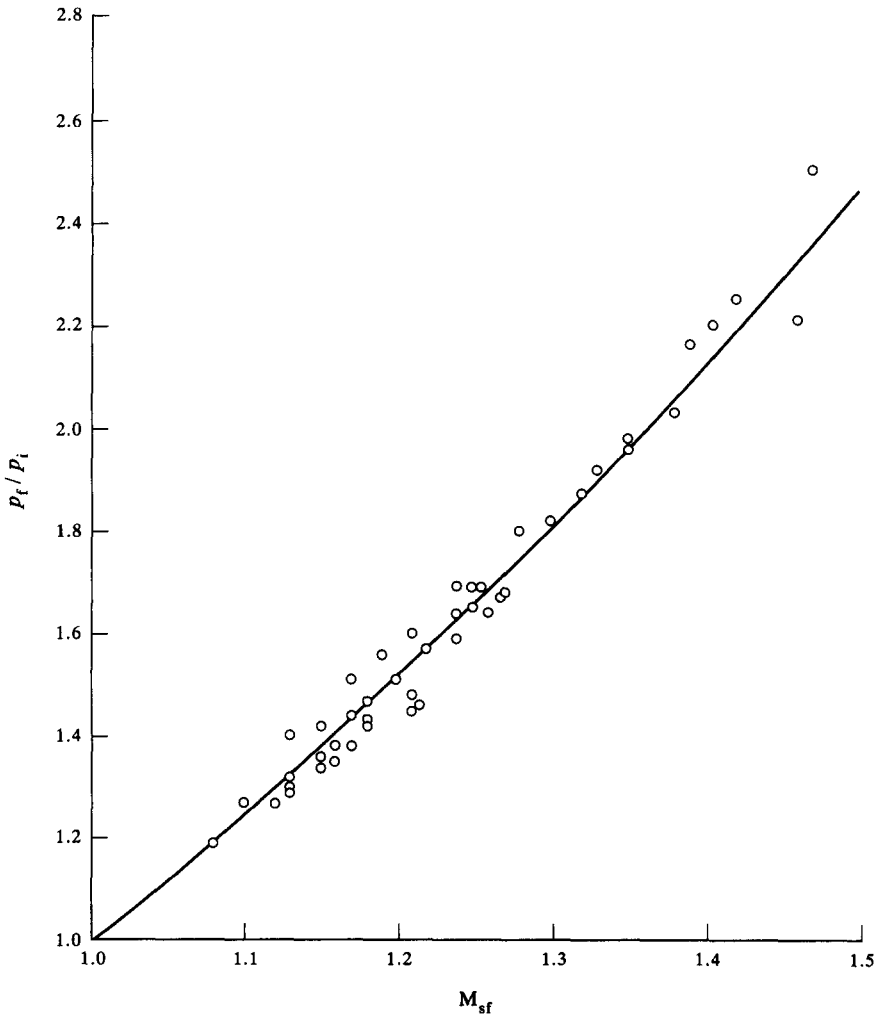

Figure 5. Pressure ratio across the shock front of a normal shock wave in a dusty gas as a function of the frozen-flow shock Mach number; ——, prediction from [5].

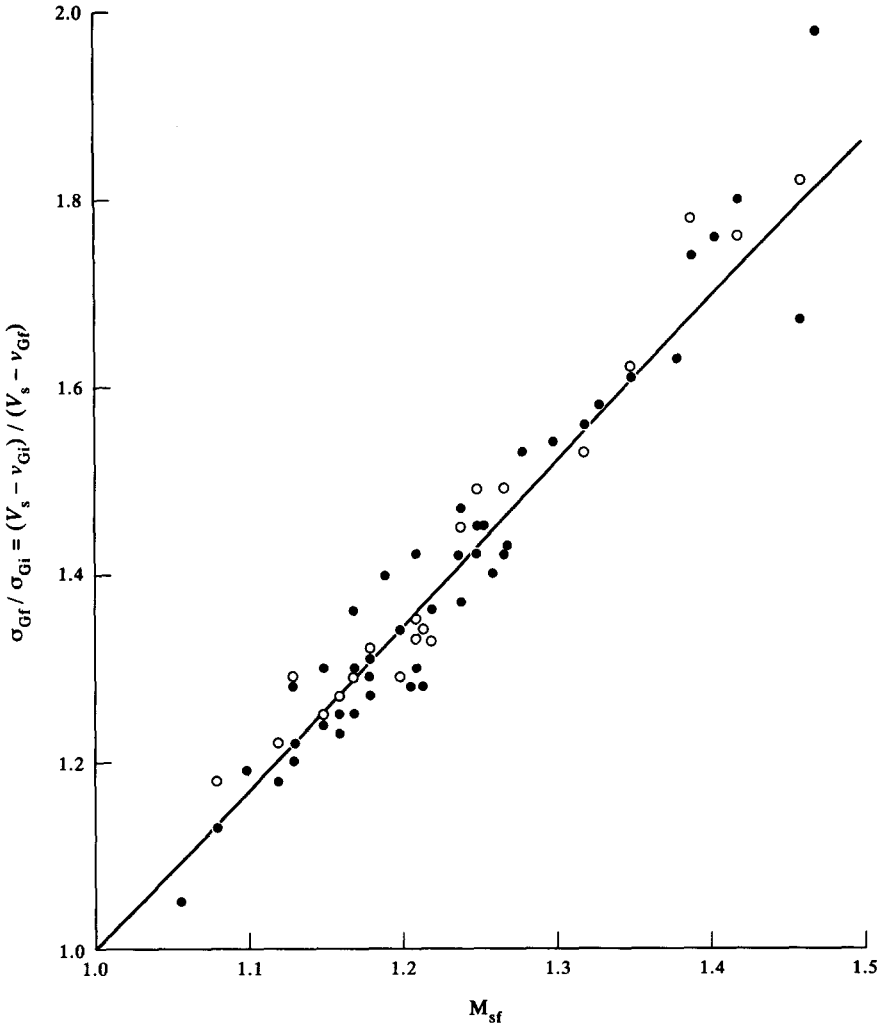

Figure 6. Gas concentration ratio (○) and gas velocity ratio (●) across the shock front of a normal shock wave in a dusty gas as a function of the frozen-flow shock Mach number; ——, prediction from [4].

The pressure history was digitized (open circles) from polaroid film records. The solid line through these points is a curve fit to the digitized data. These pressure measurements clearly exhibit the initial equilibrium region ($t < 0$), the sudden change in the gas pressure across the frozen shock front ($t = 0$), the non-equilibrium relaxation region ($t < 4$ ms) and the following equilibrium state. The final equilibrium flow pressure computed from two-phase theory, [9], is marked as p_e and shown to agree well with the experimental results.

Also shown in figure 9a (dotted line) is the profile predicted numerically from Gottlieb & Coskunses (1985). One observes that the pressure predicted numerically using these standard drag and heat-transfer coefficients rises less rapidly between the frozen and equilibrium states than the experimentally measured values. Furthermore, the predicted relaxation time (and corresponding relaxation length) is longer than the experimentally observed one.

Typical concentration measurements for the mixture (σ_m^{app}), particulate phase (σ_p) and gas phase (σ_G) are presented in figure 9b. The original data were measured with the light extinctiometer and β-ray densitometer in the dusty-gas shock tube to obtain σ_p and σ_m^{app}, and σ_G was obtained by the method outlined earlier. Although the signals from these instruments were passed through a 10 kHz low-pass filters before they were digitally recorded by the data-acquisition system, they still contain significant levels of noise. This is typical of results measured from such instruments. Hence, the concentration results were heavily smoothed by additional digital filtering, and these are the final results in figure 9b.

The concentration measurements clearly exhibit the initial equilibrium region ($t < 0$), the sudden

change in the mixture and gas-phase concentration across the shock front ($t = 0$), the subsequent relaxation region ($0 < t < 2.5$ ms) and the following final equilibrium state. The shock front does not appear as a discontinuity for the gas-phase and mixture concentrations, due partly to the finite size of the β-ray source, partly to the slow response time of the instrument and partly to the heavy numerical filtering. This response time is small compared to the relaxation time. The final equilibrium flow concentrations can be computed from [7] and known initial conditions and are marked on the figure; they agree well with the measured values.

Typical measurements of the gas- and particulate-phase velocities in a dusty-gas flow induced by a normal shock wave are summarized in figure 9c. The particulate-phase velocities measured directly by means of the LDV are presented as open circles in these plots. The gas- and particulate-phase velocities obtained indirectly by means of the measured concentrations of the gas and particulate phases, [11] and [12], are given as the solid and dotted lines, respectively. The gas-phase velocity obtained indirectly by means of [13] is given by the dashed line. The gas- and particulate-phase velocities predicted numerically are shown by the dotted-dashed lines in this figure.

These velocity measurements show clearly the initial equilibrium region with the injected dusty-air velocity of about 28 m/s ($t < 0$), the gas velocity jump at the frozen shock front ($t = 0$), the non-equilibrium relaxation zone where the gas and particulate velocities differ ($0 < t < 5$ ms)

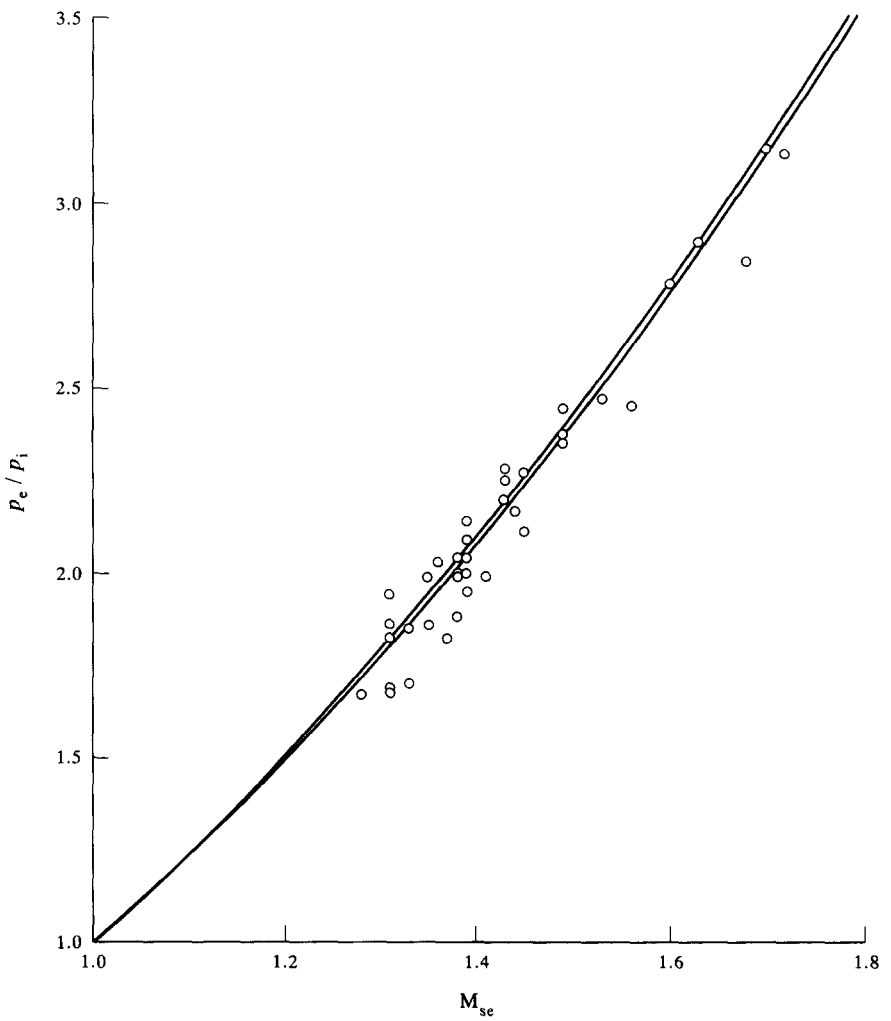

Figure 7. Pressure ratio between the final and initial equilibrium regions of a normal shock wave in a dusty gas as a function of the equilibrium-flow shock Mach number; ——, predictions from [9] for $\eta = 0.15$ (lower line) and $\eta = 0.3$ (upper line).

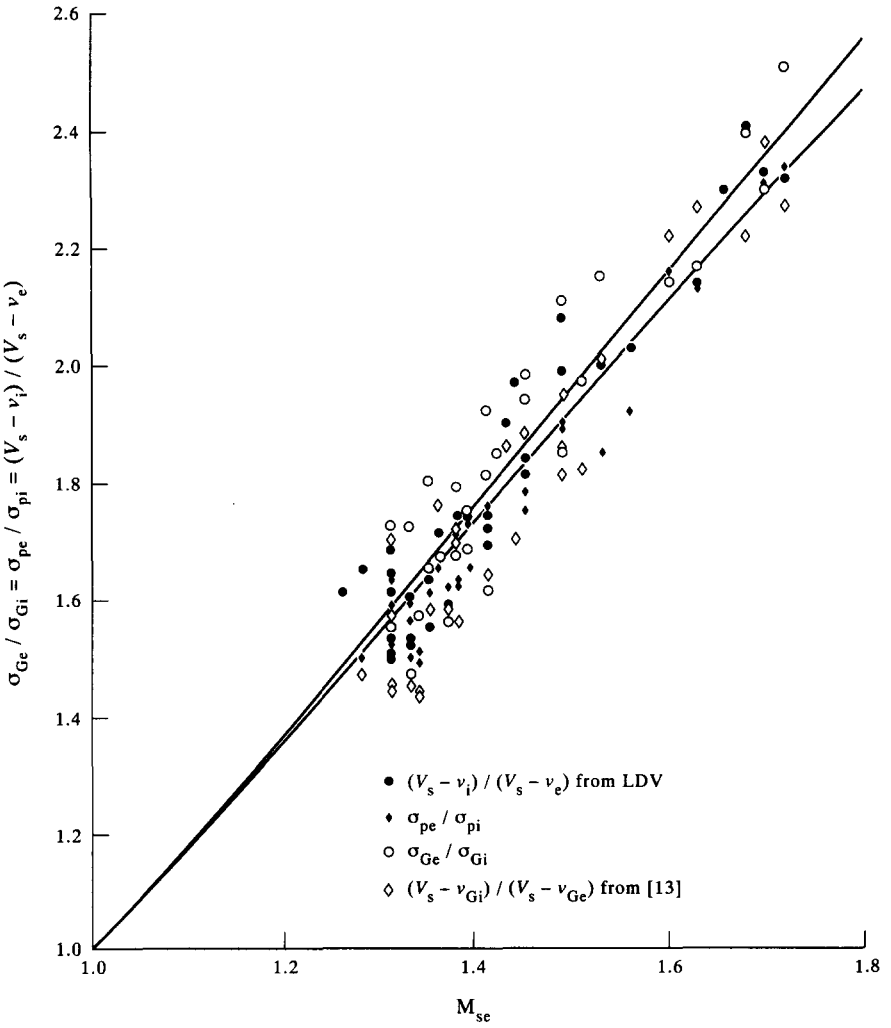

Figure 8. Gas- and particulate-phase velocity and concentration ratios between the final and initial equilibrium regions of a normal shock wave in a dusty gas as a function of the equilibrium-flow shock Mach number; ——, predictions from [7] for $\eta = 0.15$ and 0.3.

and the final equilibrium state. The equilibrium velocity of the mixture (v_e), calculated from [7], is also shown in this figure.

The gas-phase velocities obtained independently by means of [11] and [13], given by the solid and dashed lines, were generally in good agreement over most of the relaxation period. Differences between the gas velocities calculated from the different indirect methods is due mainly to experimental uncertainty. The gas velocities obtained by means of the gas concentration, [11], were found to be more reliable as they depended upon a less indirect method.

The LDV measured data shown in the velocity history exhibit scatter, partly because the dust sample includes particles of different sizes (see figure 4). Smaller particles are accelerated more quickly than large ones by viscous drag effects, and LDV samplings of such particles will exhibit larger velocities, laying closer to the indirectly measured gas-phase velocities. Additional scatter is thought to be due to the effects of flow turbulence, particle–particle collisions and the interactions of particle wakes on particle trajectories. Although one might initially expect that the LDV data should be symmetrically distributed about the dotted line (i.e. straddling it), so that the direct and indirect particulate-phase velocities should agree on some average basis, the LDV data is shifted slightly upwards from this dotted line. The velocities obtained indirectly by means of the light extinctiometer and β-ray densitometer yield *mass-averaged* velocities for the particle diameter dispersion, based on the $\tilde{\zeta}(D)$ distribution given in figure 4, whereas the direct LDV particulate velocities yield *particle-number* averaged velocities based on the $\tilde{N}(D)$ distribution. Since there is

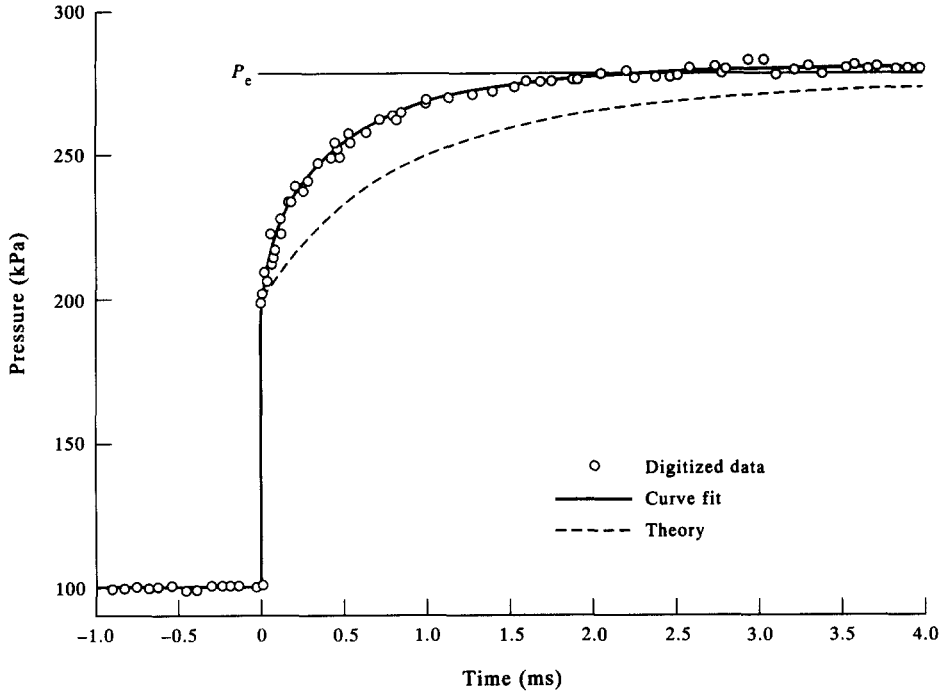

Figure 9a. Pressure measurements for a normal shock wave moving in a dusty gas ($M_{sf} = 1.36$, $M_{se} = 1.60$, $\eta = 0.27$).

a significant number of small particles present in the dust samples, this effect produces a slight upward shift of the LDV data relative to the solid line. The degree of this shift depends upon the number of small particles present in the dust sample and the *gain* setting of the LDV electronics. This is discussed in Lock & Gottlieb (1990).

Towards the end of the non-equilibrium relaxation region all measured velocities merge, with

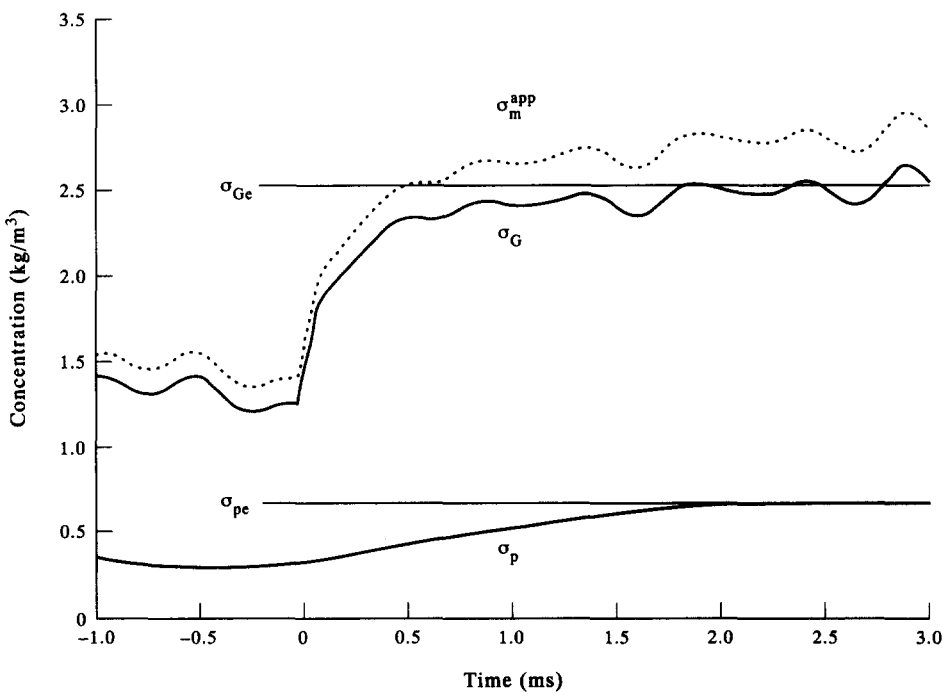

Figure 9b. Gas-phase, particle-phase and mixture concentration measurements for a normal shock wave moving in a dusty gas ($M_{sf} = 1.36$, $M_{se} = 1.60$, $\eta = 0.27$, $\Gamma = 1.28$).

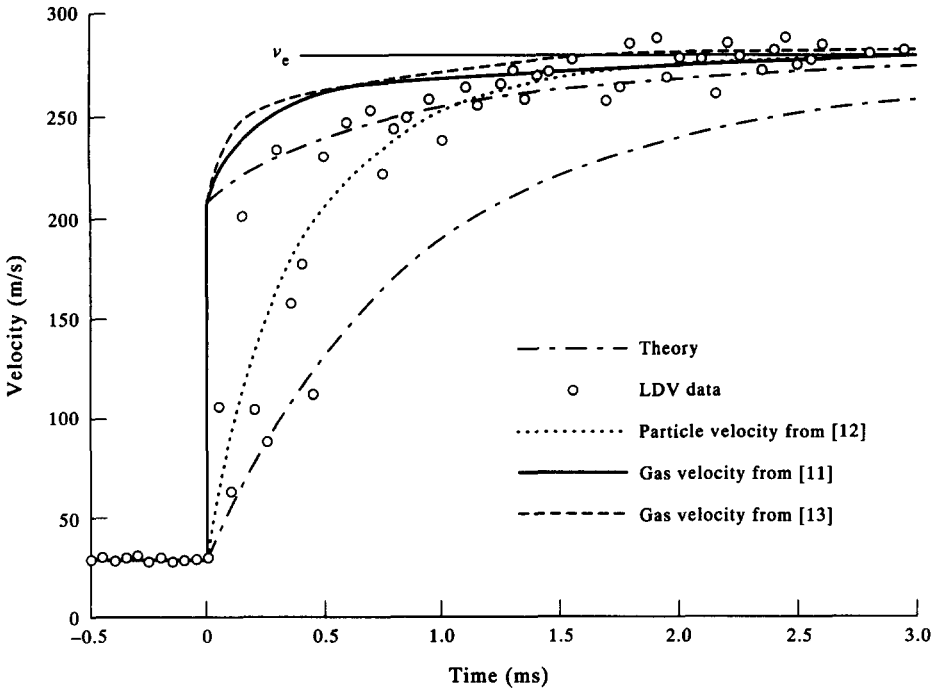

Figure 9c. Gas- and particulate-phase velocity measurements for a normal shock wave moving in a dusty gas ($M_{sf} = 1.36$, $M_{se} = 1.60$, $\eta = 0.27$, $\Gamma = 1.28$).

the exception of scatter, and the measured equilibrium data are in good agreement with the predicted equilibrium velocity, v_e. The gas- and particulate-phase velocities obtained numerically rise less quickly than the experimentally observed values. Also, the predicted relaxation times (and corresponding relaxation lengths) are longer than those observed experimentally.

Drag coefficient

The drag coefficient for a single spherical particle of diameter D is given by Newton's second law of motion:

$$C_d = \frac{4D\rho_p}{3\rho_G(u_G - u_p)^2}|\theta_p|, \qquad [14]$$

where θ_p is the acceleration of the particle along its path. This equation expresses the drag coefficient in terms of quantities which can be determined experimentally. To obtain the particle acceleration, curve fits are applied to data (such as those shown in figure 9) so that differentiation with respect to time can be performed analytically. The quantity obtained in this manner is the partial derivative $\partial v_p/\partial t$ at a fixed laboratory coordinate x, which is related to the particle acceleration for a shock with constant velocity and stationary structure as follows:

$$|\theta_p| = \frac{\partial v_p}{\partial t}\left(\frac{v_p}{V_s}\right). \qquad [15]$$

A curve fit through the experimental results (averaged from 10 experiments ranging between $1.08 < M_{sf} < 1.47$ and $1.25 < M_{se} < 1.71$) is shown in figure 10, where the drag coefficient is plotted as a function of the Reynolds number (Re). This correlation is represented by the following equation:

$$\log_{10} C_d = 0.362(\log_{10} \mathrm{Re})^2 - 2.67 \log_{10} \mathrm{Re} + 4.42. \qquad [16]$$

Also shown in this figure are the correlations obtained experimentally by Rudinger (1963, 1970) and the standard drag curve, which is the modified Henderson correlation for a relative Mach number of zero.

The experimentally deduced correlation was found to be substantially steeper than the standard

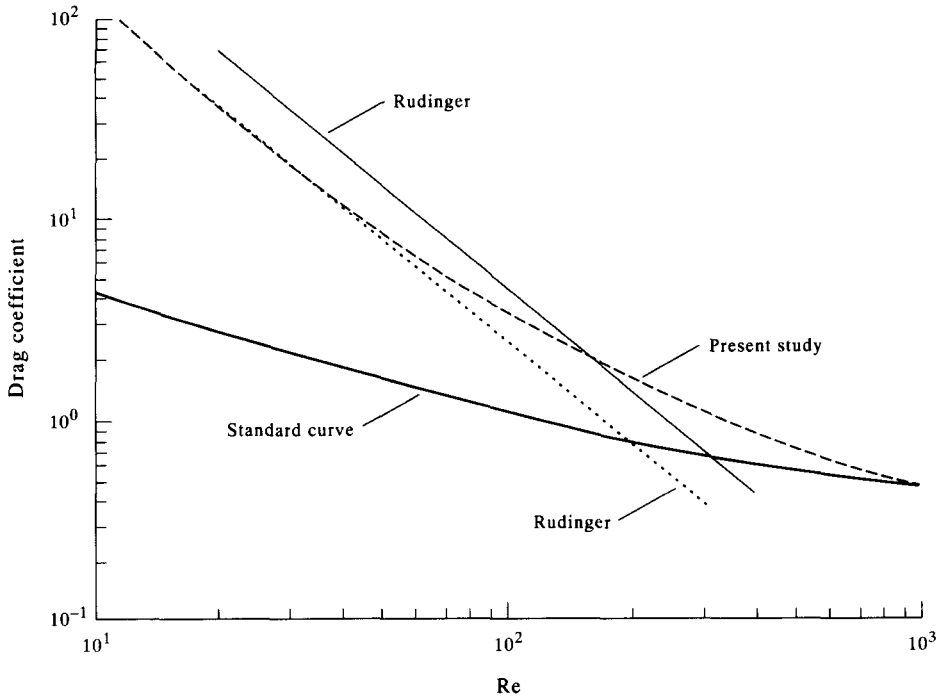

Figure 10. Drag coefficient for spheres vs Re.

or single-particle drag curve, but approached it at Re values of several hundred. The discrepancy between the experimental curves and the standard curve has been observed to become more marked as the Re decreased. Rudinger's two correlations are for particles with average diameters of 29 and 62 μm and the experimental results presented here using 40 μm generally fall between these curves.

This steep correlation is consistent with results obtained by other researchers using dusty-gas shock tubes (Buckley 1970; Selberg & Nicholls 1968; Sommerfeld 1985; Sommerfeld & Grönig 1983; Tempkin & Kim 1980). Rudinger (1970) developed a flow model to account for the steep correlation based on longitudinal and lateral perturbations in the particle motion caused by particle–particle interactions which are absent in the standard or single-particle drag curve.

CONCLUSIONS

A dusty-gas shock tube has been used to experimentally investigate the flow created by shock waves in a dusty gas. An LDV, a β-ray densitometer, a light extinctiometer and pressure transducers have been used in conjunction with indirect measurement techniques to obtain direct and indirect measurements of the gas- and particulate-phase flow properties throughout the non-equilibrium region induced by the passage of a normal shock wave with a stationary shock structure. Results of these experiments show that the thermodynamic variables follow the trends predicted by two-phase theory, but generally reach equilibrium in a shorter relaxation time than that predicted by computations using the standard drag coefficient. Measurements of the changes in the gas-phase properties across the normal shock front (frozen-flow conditions) and in the final equilibrium region have been made and are shown to be in good agreement with two-phase theory. Measurements of the drag coefficient, when correlated with the Re, have been shown to agree with those of other researchers using dusty-gas shock tubes.

Acknowledgements—The work presented in this paper was performed under the supervision of Professor J. J. Gottlieb at the University of Toronto Institute for Aerospace Studies (UTIAS). The author is grateful for the assistance of Messrs R. L. Deschambault, Z. H. Cao, J. Z. Shen and V. Levinson. The author would like to thank Professor R. C. Tennyson (Director of UTIAS) for permission to publish this work.

REFERENCES

BATT, R. G., KULKARNEY, V. A., BEHRENS, H. W. & RUNGALDIER, H. 1987 Shock induced boundary layer dust lofting. In *Proc. 16th Int. Symp. on Shock Waves and Shock Tubes*, Aachen, Germany, pp. 209–215.

BUCKLEY, F. T. 1970 Drag measurements on particles in compressible flow by a light extinction method. *AIAA Jl* **8**, 1153–1155.

CARRIER, G. F. 1958 Shock waves in dusty gases. *J. Fluid Mech.* **4**, 376–382.

CLIFT, R., GRACE, J. R. & WEBER, M. E. 1978 *Bubbles, Drops and Particles*. Academic Press, New York.

CZERWINSKI, W., DESCHAMBAULT, R. L. & LOCK, G. D. 1987 Design of a dusty-gas shock-tube facility with preliminary experimental results. UTIAS Technical Note No. 263, Univ. of Toronto, Downsview, Ontario.

DURST, F. & RUCK, B. 1987 Effective particle size range in laser-Doppler anemometry. *Expts Fluids* **5**, 305–314.

FUNK, J. F. & SAINT, D. H. 1984 A system for measuring total density in dusty shock waves using the beta attenuation technique. In *Proc. 30th Int. Instrumentation Symp.*, Denver, CO, pp. 663–676.

GOTTLIEB, J. J. & COSKUNSES, C. E. 1985 Effects of particle volume on the structure of a partially dispersed normal shock wave in a dusty gas. UTIAS Report No. 295, Univ. of Toronto, Downsview, Ontario.

HENDERSON, C. B. 1978 Drag coefficient of spheres in continuum and rarefied flows. *AIAA Jl* **14**, 707–708.

HONGRU, Y., JIANGMIN, L., SHENGXUE, Y., & ZHONGFA, L. 1985 Experimental observation of the structure of shock waves in a dusty gas. Report FTD-ID(RS)T-1262-85.

INGEBO, R. D. 1956 Drag coefficient for droplets and solid spheres in clouds accelerating in air streams. Report NACA TN 3762.

KRIEBEL, A. R. 1964 Analysis of normal shock waves in particle laden gas. *Trans. ASME J. Bas. Engng* **86D**, 655–665.

LOCK, G. D. 1991 An experimental investigation of the structure of a normal shock wave in a dusty gas. Ph.D. Thesis, Univ. of Toronto, Downsview, Ontario.

LOCK, G. D. & GOTTLIEB, J. J. 1989 Gas density and particle concentration measurements in shock-induced dusty-gas flows. Paper presented at the *17th Int. Symp. on Shock Waves and Shock Tubes*, Bethlehem, PA.

LOCK, G. D. & GOTTLIEB, J. J. 1990 Gas and particle density velocity measurements in shock-induced dusty-gas flows. Paper presented at the *5th Int. Symp. on Applications of Laser Techniques to Fluid Mechanics*, Lisbon.

MARBLE, F. E. 1970 Dynamics of dusty gases. *A. Rev. Fluid Mech.* **2**, 397–446.

MIURA, H. & GLASS, I. I. 1982 On a dusty gas shock tube. *Proc. R. Soc. Lond.* **A382**, 373–388.

MIURA, H. & GLASS, I. I. 1983 On the passage of a shock wave through a dusty-gas layer. *Proc. R. Soc. Lond.* **A385**, 85–105.

MIURA, H. & GLASS, I. I. 1985 Development of the flow induced by a piston moving impulsively in a dusty gas. *Proc. R. Soc. Lond.* **A397**, 295–309.

OUTA, E., TAJIMA, K. & MORII, H. 1976 Experiments and analyses on shock waves propagating through a gas–particle mixture. *Bull. JSME* **19**, 384–394.

OUTA, E., TAJIMA, K. & SUZUKI, S. 1981 Cross-sectional concentration of particles during shock process propagating through a gas–particle mixture in a shock tube. In *Proc. 13th Int. Symp. on Shock Waves and Shock Tubes*, Albany, NY, pp. 655–663.

RITZEL, D. V. 1985 Blast wave density measurements. In *Proc. 15th Int. Symp. on Shock Waves and Shock Tubes*, San Francisco, CA, pp. 580–585.

RUDINGER, G. 1983 Experiments on shock relaxation in particle suspensions in a gas and preliminary determination of particle drag coefficients. In *Proc. ASME Multi-phase Flow Symp.*, New York, NY, pp. 55–61.

RUDINGER, G. 1964 Some properties of shock relaxation in gas flows carrying small particles. *Phys. Fluids* **7**, 658–663.

RUDINGER, G. 1965 Some effects of finite particle volume on the dynamics of gas–particle mixtures. *AIAA Jl* **3,** 1217–1222.

RUDINGER, G. 1970 Effective drag coefficient for gas–particle flow in shock tubes. *Trans. ASME J. Bas. Engng* **92D,** 165–172.

RUDINGER, G. 1980 *Fundamentals of Gas–Particle Flow.* Elsevier, Amsterdam.

SCHLICHTING, H. 1968 *Boundary-layer Theory.* McGraw-Hill, New York.

SELBERG, B. P. & NICHOLLS, J. A. 1968 Drag coefficient of small spherical particles. *AIAA Jl* **3,** 401–408.

SOMMERFELD, M. 1985 The unsteadyness of shock waves propagating through gas–particle mixtures. *Expts Fluids* **3,** 197–206.

SOMMERFELD, M. 1989 The influence of solid particles on the structure of supersonic free jet flows. Paper presented at the *17th Int. Symp. on Shock Waves and Shock Tubes*, Bethlehem, PA.

SOMMERFELD, M. & GRÖNIG, H. 1983 The decay of shock waves in a dusty gas shock tube with different configurations. In *Proc. 14th Int. Symp. on Shock Waves and Shock Tubes*, Sydney, NSW, pp. 470–477.

SOMMERFELD, M., SELZER, M. & GRÖNIG, H. 1985 Shock wave reflections in a dusty gas. In *Proc. 15th Int. Symp. on Shock Waves and Shock Tubes*, San Francisco, CA, pp. 683–689.

SOO, S. L. 1967 *Fluid Dynamics of Multiphase Systems.* Blaisdell, Lexington, MA.

SUGIYAMA, H., HATANAKA, H., TAKIMOTO, A. & SHIROTA, T. 1985 An experimental study on shock waves propagating through a dusty-gas in a horizontal channel. In *Proc. 15th Int. Symp. on Shock Waves and Shock Tubes*, San Francisco, CA, pp. 667–673.

SUZUKI, T., ADACHI, T. & KOBAYASHI, S. 1989 An experimental analysis on shock reflection over the two-dimensional model of a dust layer. Paper presented at the *17th Int. Symp. on Shock Waves and Shock Tubes*, Bethlehem, PA.

TEMPKIN, S. & KIM, S. S. 1980 Droplet drag induced by weak shock waves. *J. Fluid Mech.* **96,** 133–157.